



Improving the crystallinity and texture of oblique-angle-deposited AlN thin films using reactive synchronized HiPIMS

Journal Article

Author(s):

Patidar, Jyotish; Sharma, Amit; Zhuk, Siarhei; Lorenzin, Giacomo; Cancellieri, Claudia; [Sarott, Martin F.](#) ; [Trassin, Morgan](#) ; Thorwarth, Kerstin; Michler, Johann; Siol, Sebastian

Publication date:

2023-09-15

Permanent link:

<https://doi.org/10.3929/ethz-b-000617453>

Rights / license:

[Creative Commons Attribution 4.0 International](#)

Originally published in:

Surface and Coatings Technology 468, <https://doi.org/10.1016/j.surfcoat.2023.129719>

Funding acknowledgement:

188414 - Multifunctional oxide electronics using natural ferroelectric superlattices (SNF)
196061 - Designing oxide electronics with light (SNF)



Improving the crystallinity and texture of oblique-angle-deposited AlN thin films using reactive synchronized HiPIMS

Jyotish Patidar^a, Amit Sharma^b, Sjarhei Zhuk^a, Giacomo Lorenzin^c, Claudia Cancellieri^c, Martin F. Sarott^d, Morgan Trassin^d, Kerstin Thorwarth^a, Johann Michler^b, Sebastian Siol^{a,*}

^a Laboratory for Surface Science and Coating Technologies, Empa – Swiss Federal Laboratories for Materials Science and Technology, Switzerland

^b Laboratory for Mechanics of Materials and Nanostructures, Empa – Swiss Federal Laboratories for Materials Science and Technology, Switzerland

^c Laboratory for Joining Technologies and Corrosion, Empa – Swiss Federal Laboratories for Materials Science and Technology, Switzerland

^d Department of Materials, ETH, Zürich, Switzerland

ARTICLE INFO

Keywords:

HiPIMS
AlN
Synchronized HiPIMS
Texture
Oblique-angle deposition

ABSTRACT

Many technologies, such as surface-acoustic-wave (SAW) resonators, sensors, and piezoelectric MEMS require highly-oriented and textured functional thin films. The best results are typically achieved for on-axis sputter geometries, but in some scenarios, this is not feasible, such as during co-deposition from multiple magnetrons or when coating substrates with high aspect ratios. Ionized physical vapor deposition (PVD) techniques such as HiPIMS can be used to accelerate the film-forming species onto the growing film using substrate-bias potentials, thus increasing adatom mobility and film texture. However, gas-ion incorporation can limit the feasibility of such synthesis approaches for defect-sensitive functional thin films. This work reports on the oblique-angle deposition of highly textured, c-axis oriented AlN (0002) films using reactive metal-ion synchronized HiPIMS. AlN thin films deposited using direct current magnetron sputtering (DCMS) and HiPIMS are discussed for comparison and the effect of ion irradiation through substrate biasing is investigated. We find that combining HiPIMS with a moderate substrate bias of only -30 V improves the crystalline quality and texture of the films significantly, while the process-gas incorporation and point defects formation can be further reduced by synchronizing the negative substrate bias potential to the Al-rich fraction of each HiPIMS pulse. In addition to a pronounced out-of-plane texture, the films show uniform polarization of the grains making this synthesis route suitable for piezoelectric applications. While the compressive stress in the films is still comparatively high, the results already demonstrate, that metal-ion synchronized HiPIMS can yield promising results for the synthesis of functional thin films under oblique-angle deposition conditions - even with low substrate-bias potentials.

1. Introduction

The functional properties of thin-film materials are often governed by their structural properties. This makes the control of microstructure and texture an important challenge in the development of functional coatings. Physical vapor deposition (PVD) techniques, such as magnetron sputtering, enable the control of the microstructure over large ranges. Depending on the process parameters, different regions in the structure zone diagram, varying from small porous crystallites to large columnar grains are accessible [1,2]. Similarly, the texture of the films can be controlled by choosing appropriate growth conditions and choice of substrates [3–5]. For many applications, highly crystalline and textured films are preferred. In piezoelectric thin films, for instance, a

pronounced and uniform out-of-plane texture of the films is necessary to achieve a high piezoelectric response [6,7].

Reports have shown, that grain growth during sputtering is strongly influenced by the direction of the incident sputter flux [8–10]. During sputtering at oblique deposition angles, grains tend to preferably grow towards the deposition source. Consequently, for the growth of out-of-plane textured thin films, the preferred sputter geometry is along the substrate normal, i.e. “on-axis”. In many deposition chamber designs, especially when co-sputtering from multiple magnetrons, on-axis deposition is not feasible. Moreover, some applications may also necessitate deposition on structured surfaces. Here, the deposition angle changes with the surface topography, which makes the growth of uniformly textured films on these substrates a particularly challenging task

* Corresponding author.

E-mail address: sebastian.siol@empa.ch (S. Siol).

<https://doi.org/10.1016/j.surfcoat.2023.129719>

Received 26 January 2023; Received in revised form 28 April 2023; Accepted 11 June 2023

Available online 17 June 2023

0257-8972/© 2023 The Authors. Published by Elsevier B.V. This is an open access article under the CC BY license (<http://creativecommons.org/licenses/by/4.0/>).

[11–13]. Rotating the substrate during the deposition can eliminate the preferred growth axis, but the continuously varying deposition angle can lead to a reduction in overall texture and crystallinity, when compared with on-axis deposited films.

Ionized PVD (IPVD) methods, particularly high-power impulse magnetron sputtering (HiPIMS) have gained interest in recent years for several applications [14–16]. IPVD techniques are characterized by their high ionization rates compared to conventional sputtering methods, which opens up exciting opportunities for process design [16–18]. HiPIMS is a type of IPVD method, in which the power to the sputtering target is applied in the form of highly energetic pulses in the micro-second range. As a consequence, it is possible to reach much higher power densities without increasing the thermal load on the target or substrate. In addition, the high plasma densities result in higher ionization fraction of the sputtered species, which can even exceed 90 % [19,20]. The abundant ions in the plasma can be accelerated on the growing film with the application of substrate bias potentials, thus achieving higher ad-atom mobility without requiring high growth temperatures, resulting in denser and often more crystalline coatings at lower temperatures [21,22]. This is particularly interesting for the deposition on temperature-sensitive substrates [23–25]. In addition, the trajectory of the ions can be altered by the bias potentials, facilitating the growth of uniform and textured films during oblique-angle deposition or on substrates with high aspect ratios [26,27]. Fig. 1 schematically shows the oblique-angle-deposition of films in direct current magnetron sputtering (DCMS) and HiPIMS with the addition of a negative substrate bias potential. Whereas the DCMS-deposited film tends to grow in the direction of the incident sputter flux, a highly oriented film is deposited with the aid of directed ion-irradiation using a negative substrate bias potential in HiPIMS. The tilting of grains in oblique-angle depositions has been previously reported in multiple works, whereas the tilt can be approximated using the empirical cosine and tangent rules [28,29].

To date, HiPIMS is mainly used for the deposition of hard coatings and metallic thin films [30]. Especially for the deposition of wear- and temperature-resistant ceramics, such as TiAlN, TiAlSiN, CrAlTiN, and CrWN, this method is well established [31–34]. During HiPIMS deposition of these types of coatings, substrate bias potentials exceeding -100 V are commonly used. The resulting high adatom mobility, as well as the subplantation of ions with high kinetic energy promote the formation of dense films and often result in mechanically stronger coatings compared to those prepared with conventional sputtering techniques

[35]. However, one of the downsides of this approach is that the negative substrate bias also accelerates the process gas ions. These ions, which are abundant in the plasma, can be implanted in interstitial sites, causing high amounts of compressive stress in the films [2,36]. This, in turn, can lead to the disorientation of grains and limit the texture of the film. The presence of such defects in the deposited films is less consequential for the mechanical properties, compared to the optoelectronic properties. By breaking the periodicity of the crystal, these defects can result in the formation of barriers for charge transport and thus reduced charge carrier mobility [37]. In addition, these defects can also act as recombination sites, reducing carrier lifetimes and breakdown potentials [38,39].

With recent developments and the introduction of novel synthesis approaches like metal-ion-synchronized HiPIMS (MIS-HiPIMS), it is now possible to selectively increase the kinetic energy of specific ions, while at the same time minimizing process gas incorporation in the films [40,41]. During HiPIMS, different sputtered species can arrive at the substrate at different times following each pulse. It has been shown previously that the gas-ions tend to arrive at the substrate nearly simultaneously with the rise in HiPIMS discharge current, however, the metal ions are generated from the target surface only after the target current density reaches higher values [19]. The impulse transferred by the sputtered atom flux also leads to a reduction in density of sputtering gas in the vicinity of the target (commonly referred to as “gas rarefaction”). Consequently, the discharge is mainly dominated by the metal-ion vapor during the later part of HiPIMS pulse [42,43]. Both, gas-rarefaction effects and differences in masses of the ionized species, can result in a different time-of-flight to the substrate. This causes a phase shift between the gas- and metal-rich parts of the sputter flux incident at the substrate, i.e. in each pulse, the gas-ions arrive before the metal-ions [44,45]. MIS-HiPIMS utilizes this effect to selectively accelerate specific species. If the arrival time of the different ions at the substrate is known, the bias potential can be pulsed accordingly to attract the metal-ion-rich part of the plasma, essentially providing the advantages of energetic ion bombardment during the film’s growth and at the same time reducing the gas incorporation and thus defects in the films. Several recent research works have shown improvements in crystallinity and texture with reduction of the gas-ion incorporation in the films with the application of synchronized HiPIMS [46–49]. This raises the question if MIS-HiPIMS approaches can be used for a wider variety of coatings, such as electroceramics or even semiconducting coatings.

In this work, we investigate the advantages of synchronized HiPIMS

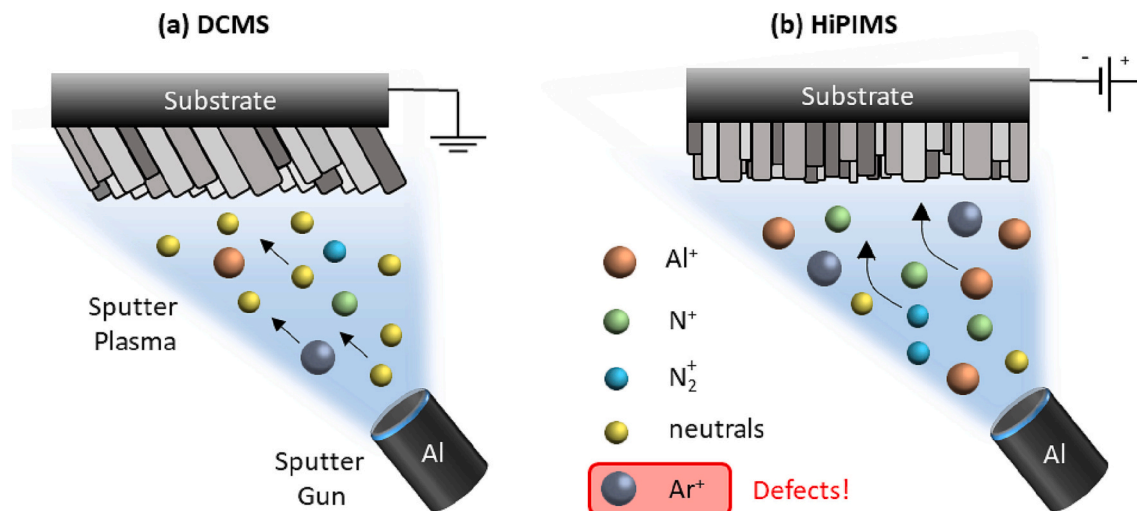


Fig. 1. Schematic representing growth of AlN films in (a) DCMS and (b) HiPIMS methods. The grains are oriented in the direction of the incident sputter flux in DCMS, while a columnar growth normal to the substrate plane can be observed in HiPIMS-deposited films using negative substrate-bias potentials due to directed ion-irradiation along the substrate normal. At the same time, acceleration and implantation of Ar^+ ions can lead to process gas incorporation in the film leading to the generation of defects.

over conventional sputtering approaches for the deposition of AlN thin films in an oblique-angle deposition geometry. Since AlN is commonly used in piezoelectric applications, the crystallographic texture is one of the most critical properties when synthesizing AlN thin films.

Aluminum nitride in wurtzite structure (space group 186, $P6_3mc$) is one of the most widely employed materials for piezoelectric applications, mainly because of its unique properties such as linear frequency response, piezoelectric stability at higher temperatures, wide band gap, and compatibility with CMOS technology [50,51]. A variety of deposition techniques have been used to produce textured AlN thin films, ranging from direct current magnetron sputtering (DCMS), HiPIMS, chemical vapor deposition, and atomic layer deposition [13,52–55]. In industrial settings, AlN is commonly synthesized using DCMS in an on-axis geometry using large targets and relatively low working distances on substrates of low surface roughness to achieve high deposition rates, a pronounced out-of-plane texture, and low compressive stress.

In this study, we synthesize AlN film in oblique-angle geometry in a confocal sputter-up geometry, as it is found in many R&D sputter chambers worldwide. Moreover, with this deposition setup, the results and their implications can also be applied to the deposition of films on structured substrates. Different approaches for the reactive sputter deposition are used, including DCMS and synchronized HiPIMS. The process optimization and development are discussed in detail, along with an in-depth characterization of the resulting film properties. The films deposited using HiPIMS show an enhanced texture and orientation compared to the DCMS films deposited with similar conditions. The effect of low energy ion-irradiation is investigated by working with small substrate-bias voltages to reduce the amount of defects, which are crucial for piezoelectric applications. Furthermore, the application of synchronized substrate biasing is investigated. XRD measurements show

a strongly pronounced c-axis orientation, whereas piezoresponse force microscopy confirms a uniform polarization of the grains, which highlights the promise of MIS-HiPIMS for the deposition of piezoelectric thin films.

2. Methods

AlN thin films were deposited using DCMS and HiPIMS in a commercial, custom-built sputter chamber (AJA International, ATC-1800), as shown in Fig. 2. The system has four sputter guns arranged in a confocal sputter-up geometry. The depositions were carried out on p-type (001) Si wafers from a single unbalanced magnetron equipped with a 2 in. Al target (HMW Hauner, purity: 99.999 at.%) with a sputter angle of 26° (with respect to the substrate normal) and a working distance of 12 cm. The substrates were ultrasonically cleaned in acetone and ethanol before the deposition. A base pressure of $<1 \times 10^{-6}$ Pa was achieved before the deposition to ensure minimal contamination from the chamber during the deposition. The films were deposited at a time-averaged power of 100 W and 0.3 Pa working pressure. The chamber is equipped with a set of diverter valves (supporting information Fig. S1) through which the gases can be routed to specific sputter guns. Based on the hysteresis studies (in supporting information Fig. S2), the working gas, Ar, was routed away from the active sputter gun and the reactive gas, N_2 , to the sputter gun. The substrate temperature was maintained at 280°C throughout the deposition. Substrate rotation of approx. 15 rpm was used to ensure uniform deposition. The deposition time was varied for DCMS and HiPIMS samples to facilitate similar thicknesses of the films.

In plasma-based physical vapor deposition processes, phase formation and nucleation can be greatly influenced by changes in the magnetic

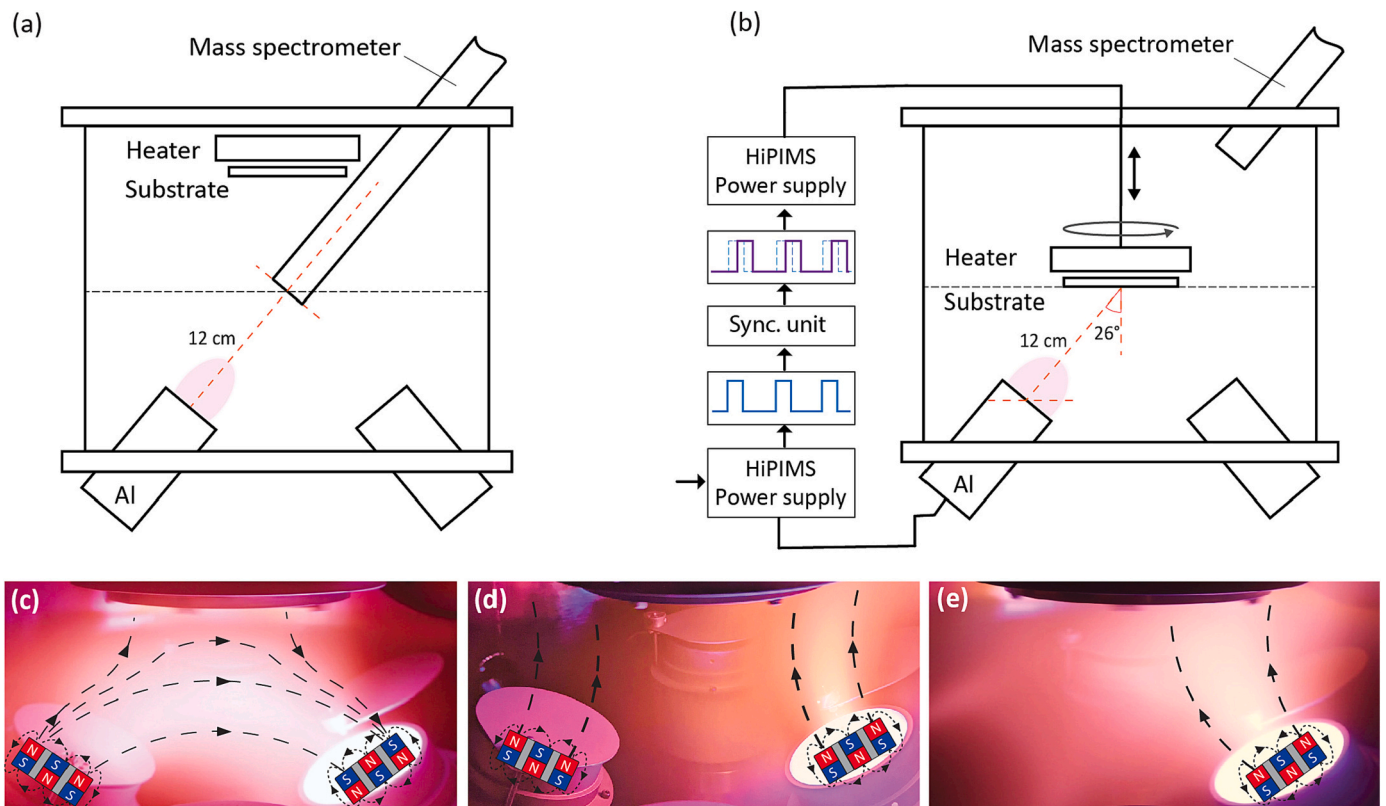


Fig. 2. Schematic of the chamber used in this study. (a) The chamber is equipped with a mass spectrometer, which is moved to the working distance to perform time- and energy-resolved measurements of the incident ions. (b) The spectrometer is retracted and the heated substrate holder is moved to perform the deposition at the same working distance. The distribution of the sputter plasma can be changed by changing the magnetic configuration in the chamber. Figures (c) and (d, e) represent the closed-field plasma and open-field plasma, respectively. The plasma distribution can be further tuned by moving the magnetron assemblies towards or away from each other (d, e).

field distribution [56–61]. In deposition systems with multiple magnetrons, the magnetic fields of different sputter guns can interact. By modifying the magnet configuration of each gun, the magnetic field distribution inside the chamber can be altered [56,62–64]. Prior to this study, we investigate two common magnetic configurations, namely, open and closed, represented in Fig. 2 (c-e). The magnetic configuration of the active magnetron was changed from a closed field (CF) to an open field (OF) configuration with the opposing counterpart, resulting in different plasma distributions in the chamber. In a CF configuration, the plasma is confined along the “closed” magnetic field lines of two magnetrons with opposite magnetic polarization. In an OF configuration, the magnetic configuration of the magnetrons is identical, so that the magnetic field lines and consequently the plasma is guided towards the substrate. For this study, all magnetrons except for the Al sputter gun and its opposite counterpart were tilted outward (i.e. towards the chamber walls) to minimize the influence of their magnetic fields. In the case of closed-field deposition, the magnetron opposite to the Al sputter gun was tilted inward (see Fig. 2c). For an open-field configuration, the angle of the opposite magnetron was adjusted in a way, so that the plasma would be directed towards the substrate position (see Fig. 2e). We evaluated the influence of the magnetic field distribution on the structural properties of the AlN thin films. The results are summarized in the supporting information S3. The crystalline quality was found to be improved with the open-field magnetic configuration due to increased ion flux towards the substrate and thus was chosen for all the subsequent depositions discussed in this investigation unless specifically stated otherwise.

The substrate holder is either grounded or negatively biased based on the different approaches followed in this work. Heating is achieved with 5 halogen lamps, resulting in homogenous temperature distribution on the substrate. The DCMS depositions were carried out using a 750 W DC power supply (AJA International, DCXS 750). HiPIMS depositions were carried out with Ionautics pulsing units and power supplies (Ionautics, HiPSTER 1 bipolar). The pulsed substrate bias was applied using the same power supplies. For the synchronization of the pulsed substrate bias potentials, the HiPIMS power supplies for the target and substrate were connected to a synchronization unit (Ionautics). The substrate potential was actively regulated to 0 V between the substrate bias pulses.

At last, the growth of AlN films without substrate rotation and at different deposition angles is demonstrated to showcase the effect of different deposition angles on the films’ growth for different deposition methods. Additional films were deposited on an etched Si wafer with substrate rotation to investigate the growth on structured surfaces.

The deposition parameters are summarized in Table 1.

The ion energy distribution functions (IEDF) of the aluminum, nitrogen, and argon positive ions were measured using an energy and time-resolved mass spectrometer (EQP-300 Hiden Analytical) (see Fig. 2b). The electrically grounded orifice (50 μm in diameter) of the instrument was placed at the working distance while facing the sputter gun. For the time-resolved measurements, the triggering signal was provided from the pulse generator of the HiPIMS power supply and used

to synchronize the measurements with the HiPIMS pulse. Ion energy distribution functions (IEDF) of 0–50 eV were measured with a delay time of 5 μs/step. The gate width (i.e. the time for which the detector collects the ions at every step) was set to 5 μs, consistent with the chosen step size. The profiling was done by measuring each ion species separately. To avoid saturation of the detector, a less abundant ³⁶Ar isotope was used for these measurements. For an accurate assessment of the ions’ time-of-flight the time of flight in the mass spectrometer needs to be considered. To calibrate this value, additional measurements were performed in which a gating potential was applied at the driven front end of the mass spectrometer. A positive potential of 25 V was applied at the driven front-end at all times, except a short 5 μs window, where the potential was reversed to –10 V. This way almost exclusively ions arriving during this short time-window are entering the mass spectrometer. The arrival time of ions on the spectrometer’s front-end was obtained by performing time-averaged measurements of the IEDFs for different gate times obtained by moving the negative –10 V pulse relative to the start of the HiPIMS discharge. The time-resolved measurement from the spectrometer was then corrected based on the arrival time of ions obtained using this technique. Using gating-potentials for time-of-flight correction, rather than calculating the time of flight in the mass spectrometer has been shown to reduce the measurement error significantly [65,66]. Further details about the method can be found in Supporting information S4.

X-ray diffraction (XRD) analysis of the films was performed using a Bruker D8 in Bragg Brentano geometry and Cu Kα radiation. Pole figures are acquired around the AlN {0002} and {10 $\bar{1}$ 3} families of planes to check the in-plane and out-of-plane texture. The pole figure scans were performed for psi angles ranging from 0° to 80° and phi from 0° to 360° with a step size of 3°. The thickness of the films was measured using a Dektak profilometer. The Ar incorporation was estimated using energy-dispersive X-ray spectroscopy (EDS) measurements performed in a Hitachi S3700 system equipped with an EDAX octane pro detector. An acceleration voltage of 5 kV was used resulting in a probing depth of about 500 nm. The thin-film stress state was evaluated using wafer curvature measurements. To this end, the Si (002) peak position was determined via rocking curve measurements in XRD on several positions on the wafer. The curvature of the substrate (R) was measured by taking the slope of the plot of measurement positions (x) against the peak position of rocking curve (ω). The residual stress (σ) in the films is measured using the Stoney equation,

$$\sigma = \frac{1}{6} \frac{E_s}{1 - \nu_s} \frac{t_s^2}{t_f} \left(\frac{1}{R} - \frac{1}{R_0} \right)$$

where E_s and ν_s are the elastic modulus and Poisson’s ratio for the Si substrate, respectively. For Si(100), the value of ($E_s/1 - \nu_s$) is 181 GPa at room temperature. t_s (≈ 0.540 mm) and t_f are the thickness of substrate and film, and R and R_0 are the curvature of wafer before and after the deposition.

The cross-sections for transmission electron microscopy (TEM) were

Table 1
Deposition parameters for DCMS- and HiPIMS-deposited AlN films in this study.

Parameter	DCMS	HiPIMS
Target-substrate distance (cm)	12	12
Sputter angle (°)	26	26
Avg. power density (W/cm ²)	~ 5	~ 5
Peak current density (A/cm ²)	0.015	0.5
Working pressure (Pa)	0.3	0.3
Ar/N ₂ flow rate (sccm)	20/10	20/10
Substrate temperature (°C)	280	280
Pulse width (μs)	–	10
Frequency (kHz)	–	7.5 kHz
Substrate bias	ground	ground/–30 V DC/40 μs pulse of –30 V (15 μs delay w. r.t. to the onset of the HiPIMS pulse)
Deposition rate (nm/min)	1.5	0.8

prepared by focused ion beam milling (Tescan, Lyra3). The STEM high-angle annular dark field (HAADF) imaging, TEM Bright field/dark field imaging, and selected-area diffraction (SAED) studies were carried out using a Themis 200 G3 aberration (probe) corrected TEM (Thermo Fischer) operating at 200 kV. Orientation imaging along the cross-section of the films was performed with scanning precession electron diffraction (SPED) technique in the TEM-based orientation imaging microscopic analysis using NanoMegas (Digital/ASTAR) having a resolution of the order of a nanometer [67]. A step size of 1 nm and a precession of 0.8° were used for all the measurements. The roughness and morphology of the films were measured using Bruker nanoscope AFM using ScanAsyst mode with silicon cantilever tips. $1 \times 1 \mu\text{m}^2$ AFM images with 512×512 pixel resolution were obtained with Nanoscope software and later processed in Gwyddion. Piezoresponse force microscopy measurements were performed using a Bruker Multimode 8 atomic force microscope, equipped with Pt-coated Si tips ($k = 5.4 \text{ N/m}$, MicroMasch). The piezoresponse was measured at a drive frequency of 10 kHz and a drive amplitude V_{AC} of 5 V.

The oxygen levels in the films were measured via depth profiling using a PHI-Quantera X-ray photoelectron spectroscopy (XPS). The XPS system is equipped with Al $K\alpha$ radiation. Charge neutralization was used throughout the measurement using a dual-beam neutralizer. The films were transferred to the XPS chamber from the deposition chamber using a custom-built UHV-transfer cart, where the pressure was maintained below 10^{-8} mbar throughout the transfer process. The XPS spectra and profiling were recorded on samples that were transferred in UHV conditions and then later exposed to the atmosphere for 5 min, to measure the oxidation in ambient conditions.

3. Results and discussion

3.1. Characterization of the HiPIMS discharge

The plasma parameters and discharge properties during the deposition play an important role in determining the growth of the film and subsequently its properties [68–70]. The plasma in the deposition chamber was first characterized using the mass spectrometer with a grounded aperture to perform measurements of the ion energy distribution function (IEDF). The IEDF of the predominant incoming ionic species present in the plasma for DCMS and HiPIMS techniques are shown in Fig. 3. While not quantitative, the difference in ion count rate is striking with HiPIMS ion count rates exceeding those of the DCMS

discharge by two orders of magnitude. The median kinetic energy of Al^+ ions is increased from approximately 6.6 eV to 10.7 eV, for DCMS and HiPIMS processes, respectively. Measurements of the N^+ ions also follow the same trend. The flux of doubly-ionized ions is also measured, however, the amount is much lower than that of singly-ionized species, and thus their effect on the films' growth is expected to be minimal. In HiPIMS, we can see different populations of ionic species for Al, Ar, and N ions in different energy ranges. The low energy peaks correspond to the background signal. The major peak and the following tail for the Al and N correspond mainly to the ions generated during the pulsed HiPIMS discharge from the nitrided surface of the target. The contribution of metal ions to the total ion flux during HiPIMS mainly depends on the pulse parameters, target state, and target current density [71,72]. The results are in good agreement with IEDFs previously reported by Jouan et al. for sputtering from an Al target, where the high energy tail is observed for HiPIMS and not for the DCMS plasma. This high energy tail is most pronounced for energetic ions generated from the target's surface, i.e. Al and N ions. In addition, due to the higher ionization rate for the HiPIMS deposition, the ion flux to the substrate is dominated by these species [73].

In order to set up the MIS-HiPIMS process, we performed measurements of the IEDF of different ions at different delay times relative to the applied HiPIMS pulse. Integrating the IEDF for each delay time, provides the ion flux as a function of time and consequently the ion's time-of-flight. Fig. 4 shows the I-U curves for the applied HiPIMS pulse on the Al target and the integrated ion fluxes of $^{36}\text{Ar}^+$ and $^{27}\text{Al}^+$ incident on the mass spectrometer. Clearly, the Ar^+ ions tend to arrive at the substrate earlier than the Al^+ ions. Based on this information, the substrate pulse is tailored to preferentially accelerate the metal ions towards the substrate. It is important to note here that the substrate bias is actively regulated to 0 V between the metal-ion-rich pulses, reducing an otherwise pronounced self-bias potential. The gas-ions incident at this time of the pulse have energies below the lattice displacement threshold, and thus the structure of the film should be primarily influenced by the ion irradiation and momentum transfer from the metal-rich part of the HiPIMS pulse [74].

3.2. Structural characterization of the films

For further investigations, we compared four representative samples deposited with different approaches, which are: AlN film deposited with DCMS and a grounded substrate, HiPIMS with a grounded substrate,

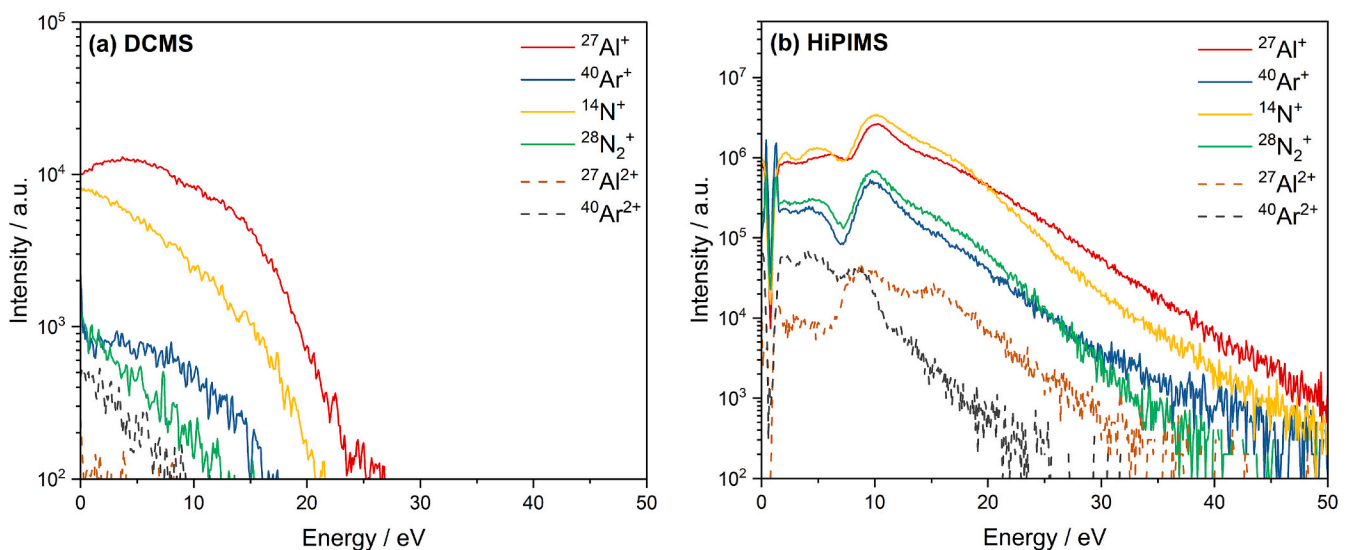


Fig. 3. Time-averaged ion energy distribution functions (IEDFs) measured for (a) DCMS and (b) HiPIMS plasma. As expected, the ion flux and kinetic energies measured in HiPIMS are significantly higher compared to DCMS.

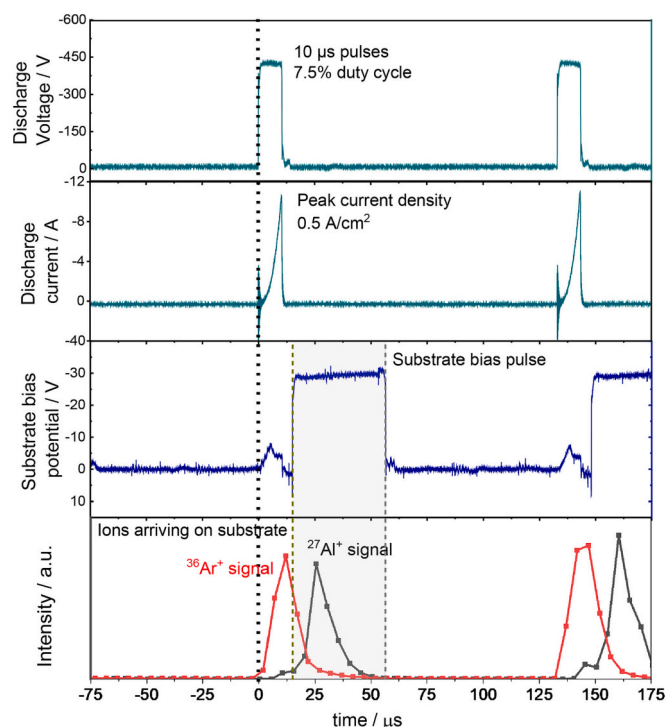


Fig. 4. Synchronization of substrate pulse with HiPIMS pulse. The substrate bias pulse is tailored to attract the metal-ions selectively for energetic metal-ion bombardment during the film growth, simultaneously avoiding gas-ion incorporation in the films.

HiPIMS with a continuous bias potential of -30 V on the substrate, as well as HiPIMS with the synchronized pulsed substrate bias potential of -30 V for a duration of 40 μ s. The bias potentials are intentionally chosen conservatively to avoid Ar-ion incorporation in the films. All samples are deposited with open field configuration and exhibit <1 at.% oxygen contamination, as measured by XPS without exposing the films to the atmosphere. For a rough estimation of the crystalline quality of the films, we used the integrated XRD intensity I_x , which is defined as the integrated area of the (0002) diffraction peak normalized by the thickness of the film. The XRD patterns, rocking curves, I_x , and the FWHM of the (0002) diffraction peak and rocking curve are plotted in Fig. 5 (a-c). A diffraction peak of the Si substrate is seen in the XRD patterns along with artifacts from residual W-K α and Cu-K β radiation due to lack on monochromator in the XRD setup.

A clear difference in the peak intensity is observed by changing the deposition method from DCMS to HiPIMS, owing to the increased ionized flux and irradiation by energetic ions. Texture coefficient is also increasing remarkably in the HiPIMS films. All HiPIMS films are nearly perfectly textured. Since four diffraction peaks are considered in the analysis, a texture coefficient of 4 would denote a completely textured film [75]. For further improvement, the energy of the impinging species during the film growth is increased by the application of substrate bias, resulting in better crystalline properties. Low energy ion-irradiation during the film growth results in higher adatom mobility, allowing the atoms to move to the lattice sites closest to equilibrium, i.e. a close-packed (0002) basal plane with the lowest surface energy [76]. This, in turn, leads to a more pronounced out-of-plane texture and a fiber texture in-plane. A shift of the (0002) diffraction peak towards lower 2θ values with increasing substrate bias indicates an increase in compressive stress in the films. This effect is most pronounced for the continuous substrate bias potential. A more detailed discussion of the stress state is given in the following section.

The rocking curve on the (0002) reflection was measured to estimate the mosaicity of samples (see Fig. 5b). The FWHM of the rocking curve is

often used as a relative measure of c-axis orientation. Here, a lower FWHM indicates fewer misaligned grains and a more coherent in-plane crystal arrangement. The FWHM of the rocking curve is seen to reduce as we move from DCMS to HiPIMS and further to continuous bias and synchronized bias, indicating an improvement in the texture of the films. In addition, for a more comprehensive assessment of the texture, XRD pole figures were recorded for the (0002) and (10 $\bar{1}$ 3) reflections (Fig. 5d). The pole figures confirm the latter results with the MIS-HiPIMS film being the most strongly oriented in (0002). The films exhibit a fiber texture, i.e. they are randomly oriented in-plane with a preferential orientation of grains normal to the plane of the substrate. The narrower intensity distribution in MIS-HiPIMS film indicates increased in-plane crystal coherency.

3.3. Stress analysis of the films

The total calculated values of stress are plotted in Fig. 6 along with the Ar incorporation in the film from EDS analysis. Here negative values of stress correspond to compressive stress in the system. All films exhibit varying amounts of compressive stress, where the highest stress values were measured for the HiPIMS depositions using substrate biasing. The measured compressive stress in the DCMS and HiPIMS deposited films are in good agreement with previous reports in literature [77,78].

In addition to the wafer curvature measurements, the stress state was also evaluated using the Crystallite Group Method (CGM) [79,80]. While the results from the CGM follow the same overall trend as the stress analysis based on wafer curvature measurements, the calculated compressive stresses are significantly larger. Similar discrepancies have been observed throughout the literature with the CGM often over-estimating the stress state when compared to wafer curvature analysis [81,82]. Due to higher accuracy and relevance, emphasis is put on these results from wafer curvature analyses. The stress analysis using the CGM can be found in supporting information S5.

Several factors contribute to stress in thin films. The most common factors are thermal, epitaxial, and intrinsic stresses. All films were deposited using a nominal substrate temperature of 280 $^{\circ}$ C. During sputtering, the actual surface temperature on the substrate surface can be significantly higher (e.g. due to plasma heating or condensation heat transfer). Assuming an additional heating of approximately 100 $^{\circ}$ C due to the applied substrate bias as well as the difference in thermal expansion coefficients for Si and AlN of $\Delta\alpha \approx 1.6^{-6}/K$, the increase in thermal stress of the films would be on the order of a few tens of MPa and therefore cannot explain the observed stress evolution. The effect of epitaxial stress is potentially larger. Valcheva et al. reported the epitaxial growth of AlN (0001) on Si (001) using reactive sputtering. Depending on the respective domain orientation of AlN a significant lattice mismatch with the underlying substrate is observed. The formation of misfit dislocations can relieve this strain to values of <1 %. However, their results indicated that the strain is predominantly tensile [83]. This stands in contrast with our observations that the films with the most pronounced in-plane orientation exhibit the highest compressive stress values. While the exact origin of the high compressive stress in the films is hard to pinpoint, the main contributing factor for the increased compressive stress in the films appears to be intrinsic. It is noteworthy, that the lower crystallinity and open columnar structure of the DCMS films provide opportunities for stress relaxation. All HiPIMS films exhibit higher crystallinity and a compact microstructure, as evidenced in later sections. The more compact microstructure is accompanied by an increase in compressive stress. However, the most striking increase in compressive stress occurs with the application of a substrate bias and therefore is likely related to the energetic ion bombardment during growth. Upon application of a substrate bias potential, the kinetic energy of the incident ions is increased by the plasma-potential drop at the substrate. Based on the median kinetic energies during HiPIMS on the order of 10 eV (see Fig. 3) this would produce a significant amount of

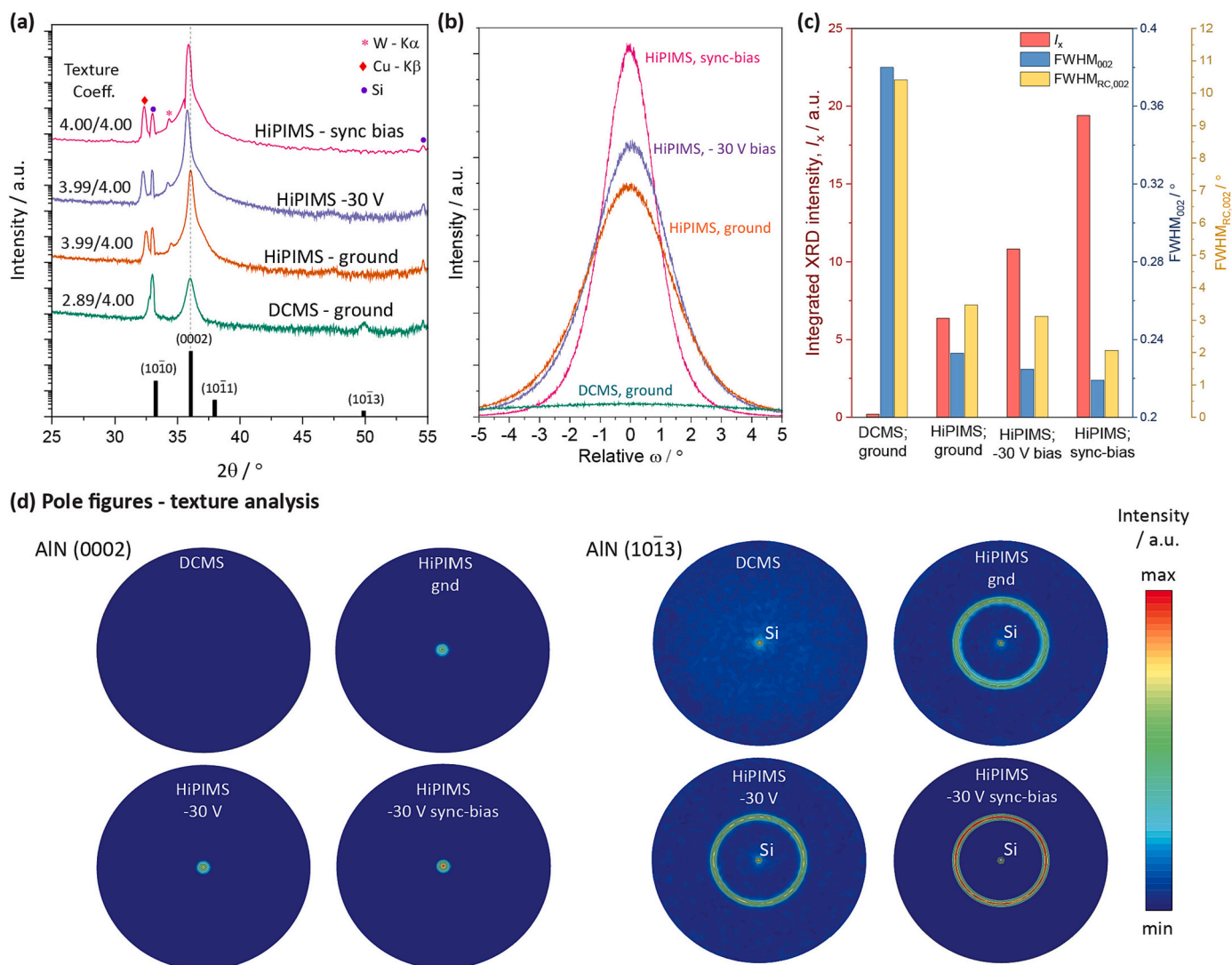


Fig. 5. Structural analysis of the representative films. (a) XRD patterns of films deposited with different approaches; (b) Normalized rocking curves; (c) Variation of integrated intensity I_x , FWHM of (0002) diffraction peak, and Ar incorporation in the deposited films. The crystalline quality is markedly improved with HiPIMS and furthermore with the application of biasing, particularly synchronized biasing. (d) XRD pole figures of the (0002) and ($10\bar{1}3$) reflections. The pole figures suggest increased out-of-plane texture in (0002) direction and random in-plane texture for the HiPIMS deposited films.

ions with kinetic energy over 40 eV, i.e. above the lattice displacement threshold [84]. This can lead to ion-implantation and structural defects in the growing films as reported by several groups [30,85]. Due to the improved crystalline quality of the HiPIMS films, the increase in stress is more likely due to ion-implantation. It was observed that the compressive stress in the films strongly correlates with Ar incorporation. In contrast to the film-forming species, the energetic Ar^+ ions from the plasma are incorporated at interstitial sites in the AlN lattice, so that even small amounts of impurities can generate a significant amount of stress in the films [49,86].

Through appropriate substrate-bias synchronization, this detrimental effect can be mitigated to some degree. While the Ar content and compressive stress in the MIS-HiPIMS film are lower than for the constant bias deposition, there is still room for further improvements by optimizing the substrate bias pulse pattern.

3.4. Microstructure analysis of the films

Transmission electron microscopy (TEM) cross-sections of the films were analyzed on focused ion beam (FIB) lamellae from the four representative samples (see Fig. 7 and Section S6 of the Supporting

Information). Bright-field TEM images are shown along with the corresponding orientation maps obtained via SPED. All AlN films exhibit a columnar structure. Grain size and texture are increased for the HiPIMS films as compared to the DCMS film, which is also visible in the SPED analysis of the respective films. The reduced grain size is in line with the lower ad-atom mobility during the DCMS process. HiPIMS films, especially those deposited with continuous and pulsed biasing show a compact columnar growth. Upon adding the substrate bias, the grain size is further increased with grains extending over the full thickness of the film.

A substantial difference in the texture of the films is evident from the in-plane and out-of-plane SPED analysis. The DCMS film exhibits generally small randomly oriented grains, while a highly oriented (0002) film can be seen for HiPIMS with synchronized biasing. While the pole figures of the AlN ($10\bar{1}3$) reflection shows no pronounced in-plane orientation, the more sensitive SPED measurement reveals a weak preferential in-plane orientation in ($2\bar{1}10$) and ($10\bar{1}0$) directions. This is well in line with the epitaxial relationship between Si (001) and AlN (0001) [83,87]. To further analyze the texture of the films, selected area electron diffraction (SAED) was performed. As expected, the DCMS film shows a randomly oriented polycrystalline structure, while the HiPIMS

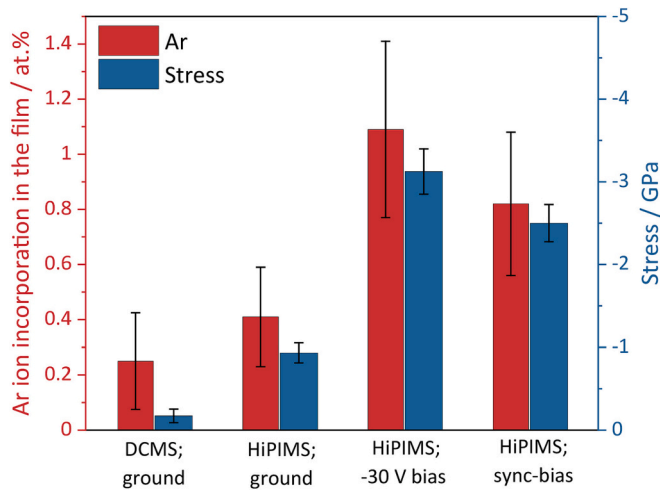
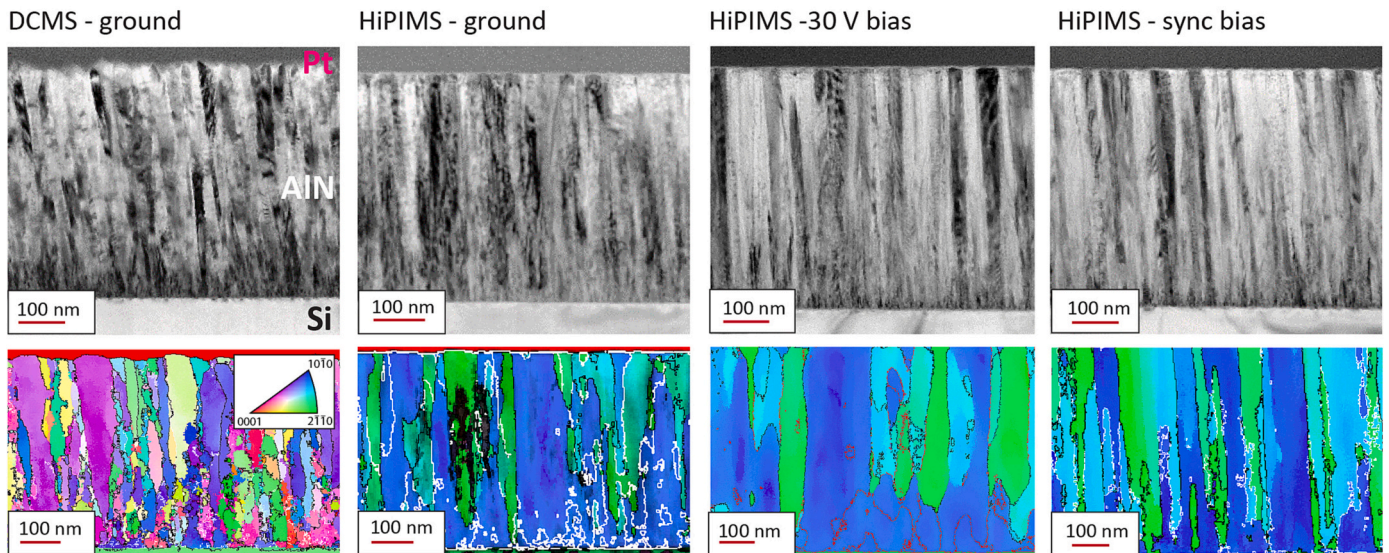


Fig. 6. Evaluation of the in-plane stress in the films deposited with different approaches. The compressive stress in the films is strongly correlated with the Ar-ion incorporation in the films. The amount of Ar incorporation in films decreases with the application of the synchronized bias.

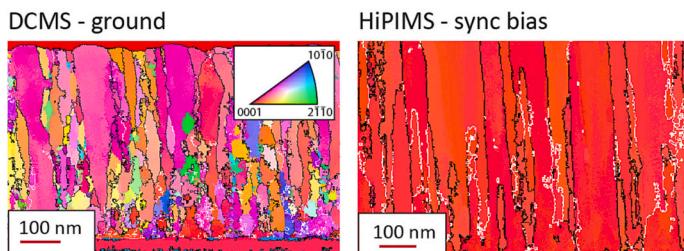
film with synchronized biasing shows a bi-axial texture along the $(2\bar{1}\bar{1}0)$ and $(10\bar{1}0)$ zone axes. It is noteworthy, that as we move from DCMS to HiPIMS and to additional substrate biasing, the kinetic energy of the film forming ions is increasing, while the nominal substrate temperature is kept constant. The more pronounced columnar growth with the increased energetic bombardment is well in line with the microstructural evolution outlined in the often referenced modified structure zone diagram [2].

The difference in microstructure is also reflected in the surface roughness, as evidenced by AFM measurements (see Fig. 8). The root mean square (RMS) roughness measured over a $1 \mu\text{m}^2$ area of the film is markedly reduced to $<1 \text{ nm}$ in HiPIMS-deposited films, in contrast to the 4 nm RMS roughness for the DCMS film. The rough surface of the films deposited with grounded substrates in both, DCMS and HiPIMS, can be seen in the bright-field TEM cross-sections as well. Furthermore, to assess the polarization of the grains, qualitative PFM measurements were performed. Both the out-of-plane and the in-plane piezoresponse images revealed no variation in contrast in all tested films (see Section S7 in supporting information). The lack of apparent piezoelectric domains indicates a uniform polarization across all grains. These results are promising and indicate, that films deposited with HiPIMS, particularly with a synchronized substrate bias, could be used for piezoelectric applications, even when deposited via oblique angle deposition or on structured surfaces.

(a) Transmission electron microscopy (TEM) and scanning precession electron diffraction (SPED) imaging



(b) out-of-plane SPED imaging



(c) SAED

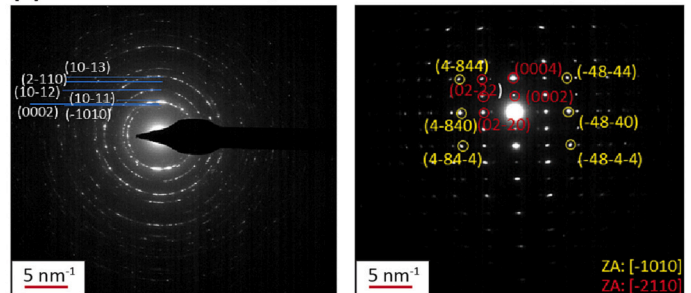


Fig. 7. (a) Bright-field and SPED TEM imaging of four representative films. The red and white colors in the IPF map (inset of SPED images) represents low and high angle grain boundaries. The HiPIMS films show a pronounced columnar growth and out-of-plane orientation which are further improved with substrate biasing. A minor in-plane texture is evident for the HiPIMS deposited films. (b) Out-of-plane SPED imaging and (c) SAED patterns for DCMS and MIS-HiPIMS films. Both analyses show remarkable improvements in texture from DCMS to synchronized HiPIMS. (For interpretation of the references to colour in this figure legend, the reader is referred to the web version of this article.)

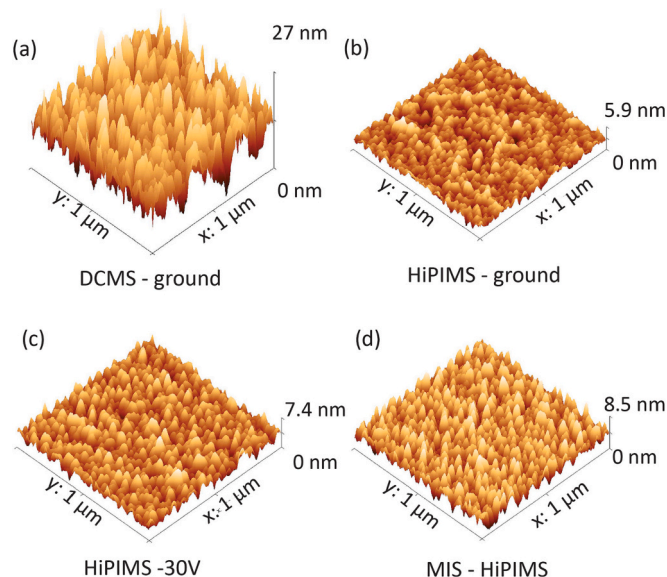


Fig. 8. Surface topography of representative samples measured using AFM. The surface roughness is evidently lower in HiPIMS samples than DCMS samples due to high ad atom mobility in the case of HiPIMS.

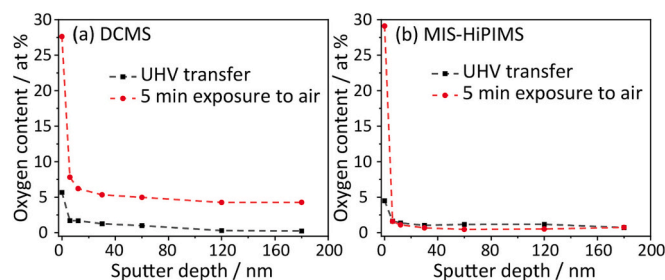


Fig. 9. Depth profiling of DCMS and MIS-HiPIMS samples done in XPS for estimation of oxygen content in the films. In the case of DCMS deposition, the increased amount of oxygen in the deeper levels of films after exposure to air indicates grain boundary oxidation. Contrary to this, the MIS-HiPIMS film shows no oxidation due to its compact columnar structure.

3.5. Surface analysis and oxidation resistance

The chemical composition of the films was analyzed via XPS combined with a UHV sample transfer, i.e. without exposing the films to the atmosphere. To probe the oxygen contamination in the films, depth profiling was performed on the samples before and after exposure to atmosphere (see Fig. 9). Both films show oxygen levels below 1 % in the film after a few minutes of sputtering. However, after performing the depth profiling on the same samples after exposure to the atmosphere, the DCMS film shows about ~5 % of oxygen levels inside the films. Contrary to this, the HiPIMS films only show surface oxidation and stay oxygen-free in the bulk of the film. This is attributed to the compact microstructure of HiPIMS films, which prevents grain boundary oxidation of the films. The oxidation resistance offered by films deposited using synchronized HiPIMS makes them particularly interesting candidates for applications in reactive environments or with limited encapsulation. In addition, it was found based on the UHV XPS experiments that the films are stoichiometric within the margin of error of the measurement. The Al/N ratio was found to be $\text{Al}_{0.45}\text{N}_{0.55}$ on the slightly

oxidized surface and $\text{Al}_{0.48}\text{N}_{0.52}$ after gentle Ar-ion milling (see supporting information, section S8). This composition was identical for DCMS and MIS-HiPIMS deposited films.

3.6. Static deposition and deposition on structured substrates– DCMS vs MIS-HiPIMS

Finally, to assess the influence of different growth modes during static deposition (i.e. without substrate rotation), the AlN films were deposited using DCMS with a grounded substrate and MIS-HiPIMS on four Si substrates placed at different positions on the substrate holder, corresponding to different incident deposition angles, as shown in Fig. 10 (a-b). A closed magnetic configuration was used, to avoid influences from non-uniform plasma heating. The preferred growth axis of the films was analyzed using a χ -scan in XRD after fixing 2θ and ω on the AlN (0002) maximum. χ is referenced to the substrate normal, i.e. a deviation of peak position from 0° indicates a tilt of grains in the film.

The DCMS films give broader peaks as compared to the MIS-HiPIMS films, indicating higher mosaicity and misalignment among the grains, in line with our expectation from the deposition using substrate rotation. Strikingly, the peak position shifts to a higher χ -angle in DCMS films as the deposition angle becomes higher. In contrast, the MIS-HiPIMS films' peaks nearly stay around 0° , indicating the growth of grain is almost normal to the substrate plane. This confirms that the energetic deposition in MIS-HiPIMS improves not only the texture of the growing film but can also be utilized to improve the out-of-plane orientation at higher sputter angles during static deposition (see Fig. 10).

To further validate this, we deposited the films on a structured wafer of Si with substrate rotation "on" throughout the deposition to ensure uniform deposition. The etched (001) Si wafer exhibits pyramids with (111) facets (see Fig. 10(c)). The χ -scan was performed (see Fig. 10(d)) by aligning the XRD on the (111) reflection of Si and optimizing ϕ (i.e. moving the (111) facets of pyramids into the diffraction plane). The deviation of the AlN peaks from the Si peak in the χ -scan effectively tells us the tilt angle of grains in the film with respect to the normal of the (111) facet. The MIS-HiPIMS films' grains show a smaller misalignment from the substrate normal and a sharper peak compared to the DCMS film. The result is in agreement with the previous investigations and is due to increased adatom mobility and bombardment of ions normal to the substrate plane. The MIS-HiPIMS film still has a small amount of grain tilt, which is supposedly due to the combination of oblique-angle deposition and the structured surface. Nevertheless, based on these results, it can be concluded that MIS-HiPIMS is a powerful tool to obtain highly oriented and textured films, irrespective of the deposition angle.

4. Conclusions

In this study, the effects of different deposition approaches and techniques, namely, DCMS and HiPIMS, were discussed to grow textured AlN (0002) films in oblique-angle deposition conditions. Specifically, we investigated if HiPIMS in combination with low negative substrate bias potentials can mitigate the detrimental effects of shallow deposition angles.

Plasma diagnostics and process parameter optimizations were conducted for DCMS and HiPIMS deposition plasmas. The effects of ion irradiation were investigated by varying the kinetic energy of the impinging ionized flux through changes in substrate bias potentials. Energy and time-resolved QMS analyses were performed to characterize the kinetic energy of major ion species in the HiPIMS process. After measuring the time-of-flight of ions following the HiPIMS pulse, the substrate bias potential was pulsed and synchronized with the HiPIMS

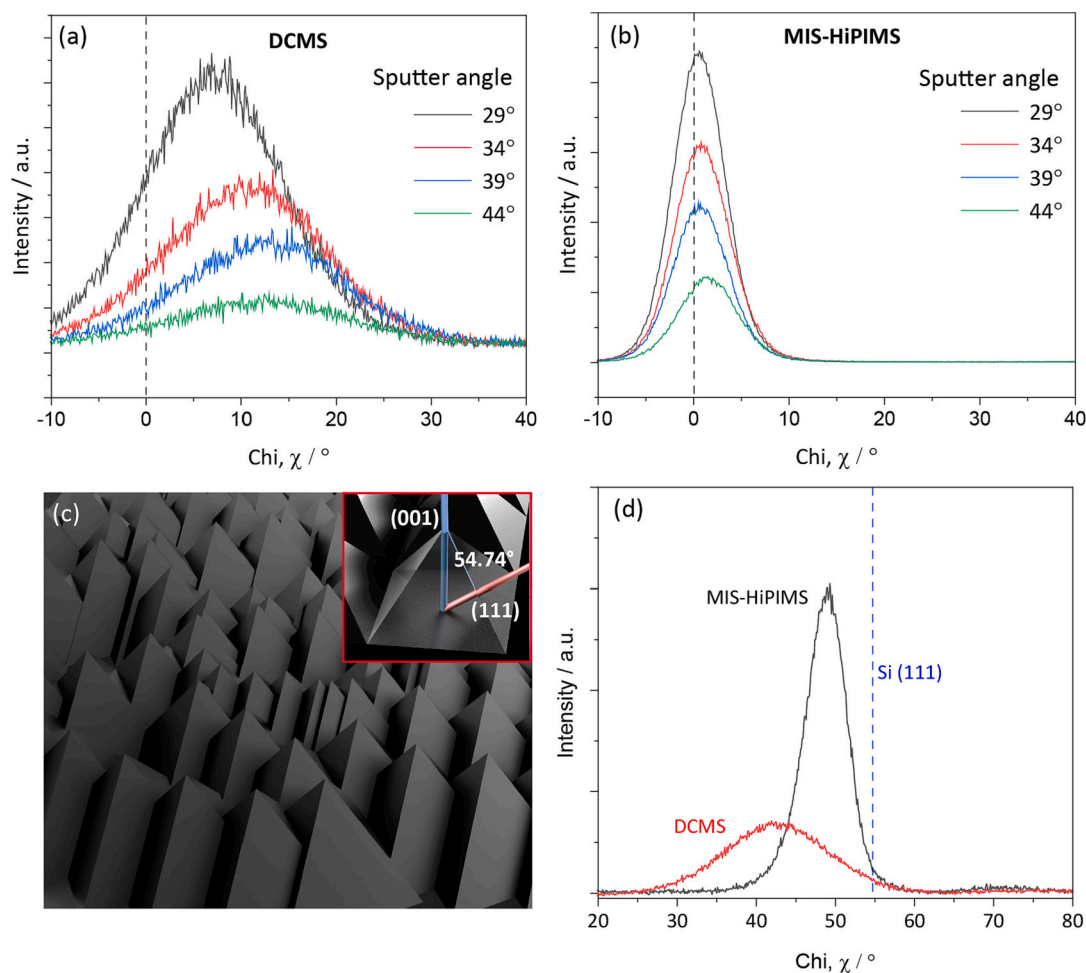


Fig. 10. Deposition of AlN films on Si substrates placed at different sputter angles (without rotating the sample holder). χ -scan for (a) DCMS (b) MIS-HiPIMS - deposited films for different sputter angles. Higher deviation in peak positions in DCMS films indicates a higher tilt of grains. The peak further shifts to a larger angle as the deposition angle increases, while the MIS-HiPIMS films stay nearly around 0° and moreover at the same position. (c) Schematic of a structured Si substrate. The substrate has micro-pyramids etched over a (001) Si wafer with (111) facets (shown in inset). (d) χ -scan for DCMS and MIS-HiPIMS film deposited on structured Si substrate with substrate rotation on. The difference of χ angle between the Si peak and AlN peaks represents the tilt of grain with respect to the Si substrate normal, which is evidently higher for DCMS film.

pulse to selectively accelerate the metal-ions on the growing film.

Four representative films grown with different approaches were chosen to compare the change in crystallinity and texture: DCMS with a grounded substrate, HiPIMS with a grounded, -30 V continuous, and a pulsed-synchronized substrate bias potential. We found that the crystalline quality and texture of the films significantly improved from DCMS to HiPIMS, owing to increased ionized flux and higher adatom mobility due to energetic ion bombardment. The quality of films was further improved by increasing the kinetic energy of impinging ions with the help of substrate biasing. The films deposited with HiPIMS were found to have low surface roughness and an evident dense columnar growth in the (0002) direction, in contrast to the DCMS film. Overall, the MIS-HiPIMS approach yielded the most promising results. Despite the low substrate bias potentials, some incorporation of Ar in the film was observed, resulting in high compressive stress. This effect, however, was reduced by applying the synchronized substrate bias potential. In addition to the improvements in crystallinity and texture, we found that a positive side effect of the compact microstructure is an improved oxidation resistance when the layers are exposed to ambient conditions.

The extent of the grain tilt in the film was estimated with the help of χ -scans in XRD. The angle at which grains are aligned with respect to the substrate normal was found to be directly correlated with the angle of sputter flux in the DCMS process. Moreover, the columnar grains in the

film stay nearly normal in MIS-HiPIMS film, irrespective of the deposition angle. These results were further validated by deposition on a structured Si substrate.

Finally, it is concluded that synchronized HiPIMS can be a promising deposition approach to synthesize films with pronounced out-of-plane texture on non-uniform substrates or in oblique deposition conditions. While more work is needed to further reduce the Ar content and consequently the compressive stress in MIS-HiPIMS mode, the presented results already demonstrate that synchronized HiPIMS processes could open up exciting opportunities for the deposition of functional defect-sensitive thin film materials in the future.

CRediT authorship contribution statement

Jyotish Patidar: Conceptualization, Investigation, Formal analysis, Visualization, Writing – original draft. **Amit Sharma:** Investigation, Formal analysis, Writing – review & editing. **Siarhei Zhuk:** Investigation, Writing – review & editing. **Giacomo Lorenzin:** Formal analysis, Writing – review & editing. **Claudia Cancellieri:** Formal analysis, Writing – review & editing. **Martin F. Sarott:** Investigation, Formal analysis, Writing – review & editing. **Morgan Trassin:** Investigation, Formal analysis, Writing – review & editing. **Kerstin Thorwarth:** Investigation, Writing – review & editing. **Johann Michler:** Writing –

review & editing. **Sebastian Siol**: Conceptualization, Supervision, Methodology, Formal analysis, Funding acquisition, Writing – review & editing.

Declaration of competing interest

The authors declare that they have no known competing financial interests or personal relationships that could have appeared to influence the work reported in this paper.

Data availability

Data will be made available on request.

Acknowledgements

The authors would like to thank Ulrich Müller for his help during the setup of the deposition chamber. Help from Monalisa Ghosh during process characterization and Alexander Wiczorek for the image design of structured Si is gratefully acknowledged. Bertrand Paviet-Salomon is gratefully acknowledged for providing the structured Si-substrates. J. P. acknowledges funding by the SNSF (project no. 200021_196980). S.Z. acknowledges funding by the Empa research commission. G.L. acknowledges the Swiss National Science Foundation (SNSF), project number 200021_192224 for financially supporting this research. M.T. acknowledges the financial support by the Swiss National Science Foundation under project No. 200021_188414. M.T. and M.F.S. acknowledge the Swiss National Science Foundation Spark funding CRSK-2_196061.

Appendix A. Supplementary data

Supplementary data to this article can be found online at <https://doi.org/10.1016/j.surfcoat.2023.129719>.

References

- [1] J.A. Thornton, Influence of apparatus geometry and deposition conditions on the structure and topography of thick sputtered coatings, *J. Vac. Sci. Technol.* 11 (4) (Jul. 1974) 666–670, <https://doi.org/10.1116/1.1312732>.
- [2] A. Anders, A structure zone diagram including plasma-based deposition and ion etching, *Thin Solid Films* 518 (15) (2010) 4087–4090, <https://doi.org/10.1016/j.tsf.2009.10.145>.
- [3] C.V. Thompson, R. Carel, Texture development in polycrystalline thin films, *Mater. Sci. Eng. B* 32 (3) (Jul. 1995) 211–219, [https://doi.org/10.1016/0921-5107\(95\)03011-5](https://doi.org/10.1016/0921-5107(95)03011-5).
- [4] A. Sharma, S. Mohan, S. Suwas, Development of bi-axial preferred orientation in epitaxial NiMnGa thin films and its consequence on magnetic properties, *Acta Mater.* 113 (Jul. 2016) 259–271, <https://doi.org/10.1016/j.actamat.2016.04.037>.
- [5] A. Sharma, S. Mohan, S. Suwas, The effect of the deposition rate on the crystallographic texture, microstructure evolution and magnetic properties in sputter deposited Ni-Mn-Ga thin films, *Thin Solid Films* 616 (Oct. 2016) 530–542, <https://doi.org/10.1016/j.tsf.2016.08.033>.
- [6] T. Yamamoto, T. Shiosaki, A. Kawabata, Characterization of ZnO piezoelectric films prepared by rf planar-magnetron sputtering, *J. Appl. Phys.* 51 (6) (Jun. 1980) 3113–3120, <https://doi.org/10.1063/1.328100>.
- [7] M.-A. Dubois, P. Mural, Stress and piezoelectric properties of aluminum nitride thin films deposited onto metal electrodes by pulsed direct current reactive sputtering, *J. Appl. Phys.* 89 (11) (Jun. 2001) 6389–6395, <https://doi.org/10.1063/1.1359162>.
- [8] H. Hajihoseini, M. Kateb, S.P. Ingvarsson, J.T. Gudmundsson, Oblique angle deposition of nickel thin films by high-power impulse magnetron sputtering, *Beilstein J. Nanotechnol.* 10 (Sep. 2019) 1914–1921, <https://doi.org/10.3762/bjnano.10.186>.
- [9] V. Elofsson, D. Magnfält, M. Samuelsson, K. Sarakinos, Tilt of the columnar microstructure in off-normally deposited thin films using highly ionized vapor fluxes, *J. Appl. Phys.* 113 (17) (May 2013) 174906, <https://doi.org/10.1063/1.4804066>.
- [10] K.R. Talley, S.L. Millican, J. Mangum, S. Siol, C.B. Musgrave, B. Gorman, A. M. Holder, A. Zakutayev, G.L. Brennecke, Implications of heterostructural alloying for enhanced piezoelectric performance of (Al,Sc)N, *Phys. Rev. Mater.* 2 (6) (Jun. 2018) 063802, <https://doi.org/10.1103/PhysRevMaterials.2.063802>.
- [11] H.L. Brown, S.A. Thornley, S.J. Wakeham, M.J. Thwaites, R.J. Curry, M.A. Baker, The impact of substrate bias on a remote plasma sputter coating process for conformal coverage of trenches and 3D structures, *J. Phys. D: Appl. Phys.* 48 (33) (Aug. 2015) 335303, <https://doi.org/10.1088/0022-3727/48/33/335303>.
- [12] A. Barranco, A. Borrás, A.R. Gonzalez-Elipe, A. Palmero, Perspectives on oblique angle deposition of thin films: from fundamentals to devices, *Prog. Mater. Sci.* 76 (2016) 59–153, <https://doi.org/10.1016/j.pmatsci.2015.06.003>.
- [13] M. Ramezani, V.V. Felmetser, N.G. Rudawski, R. Tabrizian, Growth of C-axis textured AlN films on vertical sidewalls of silicon microfilms, *IEEE Trans. Ultrason. Ferroelectr. Freq. Control* 68 (3) (Mar. 2021) 753–759, <https://doi.org/10.1109/TUFFC.2020.3013111>.
- [14] K. Sarakinos, J. Alami, S. Konstantinidis, High power pulsed magnetron sputtering: a review on scientific and engineering state of the art, *Surf. Coatings Technol.* 204 (11) (2010) 1661–1684, <https://doi.org/10.1016/j.surfcoat.2009.11.013>.
- [15] U. Helmersson, M. Lattemann, J. Bohlmark, A.P. Ehasarian, J.T. Gudmundsson, Ionized physical vapor deposition (IPVD): a review of technology and applications, *Thin Solid Films* 513 (1–2) (2006) 1–24, <https://doi.org/10.1016/j.tsf.2006.03.033>.
- [16] W.-D. Münz, M. Schenkel, S. Kunkel, J. Paulitsch, K. Bewilogua, Industrial applications of HIPIMS, *J. Phys. Conf. Ser.* 100 (8) (Mar. 2008) 082001, <https://doi.org/10.1088/1742-6596/100/8/082001>.
- [17] G. Eichenhofer, I. Fernandez, A. Wennberg, Industrial use of HiPIMS up to now and a glance into the future, a review by a manufacturer introduction of the hiP-V hiPlus technology, *Univers. J. Phys. Appl.* 11 (3) (Jun. 2017) 73–79, <https://doi.org/10.13189/ujpa.2017.110301>.
- [18] J.T. Gudmundsson, N. Brenning, D. Lundin, U. Helmersson, High power impulse magnetron sputtering discharge, *J. Vac. Sci. Technol. A Vacuum, Surfaces, Film.* 30 (3) (May 2012) 030801, <https://doi.org/10.1116/1.3691832>.
- [19] K. Macák, V. Kouznetsov, J. Schneider, U. Helmersson, I. Petrov, Ionized sputter deposition using an extremely high plasma density pulsed magnetron discharge, *J. Vac. Sci. Technol. A Vacuum, Surfaces, Film.* 18 (4) (Jul. 2000) 1533–1537, <https://doi.org/10.1116/1.582380>.
- [20] V. Kouznetsov, K. Macák, J.M. Schneider, U. Helmersson, I. Petrov, A novel pulsed magnetron sputter technique utilizing very high target power densities, *Surf. Coatings Technol.* 122 (2–3) (Dec. 1999) 290–293, [https://doi.org/10.1016/S0257-8972\(99\)00292-3](https://doi.org/10.1016/S0257-8972(99)00292-3).
- [21] L. Wang, L. Li, X. Kuang, Effect of substrate bias on microstructure and mechanical properties of WC-DLC coatings deposited by HiPIMS, *Surf. Coatings Technol.* 352 (Oct. 2018) 33–41, <https://doi.org/10.1016/j.surfcoat.2018.07.088>.
- [22] Z. Wang, D. Zhang, P. Ke, X. Liu, A. Wang, Influence of substrate negative Bias on structure and properties of TiN coatings prepared by hybrid HIPIMS method, *J. Mater. Sci. Technol.* 31 (1) (Jan. 2015) 37–42, <https://doi.org/10.1016/j.jmst.2014.06.002>.
- [23] P.J. Kelly, P.M. Barker, S. Ostovarpour, M. Ratova, G.T. West, I. Iordanova, J. W. Bradley, Deposition of photocatalytic titania coatings on polymeric substrates by HiPIMS, *Vacuum* 86 (12) (Jul. 2012) 1880–1882, <https://doi.org/10.1016/j.vacuum.2012.05.003>.
- [24] J. Mun, H. Park, J. Park, D. Joung, S.-K. Lee, J. Leem, J.-M. Myoung, J. Park, S.-H. Jeong, W. Chegal, S. Nam, S.-W. Kang, High-mobility MoS₂ directly grown on polymer substrate with kinetics-controlled metal-organic chemical vapor deposition, *ACS Appl. Electron. Mater.* 1 (4) (Apr. 2019) 608–616, <https://doi.org/10.1021/acsaelm.9b00078>.
- [25] S. Loquai, B. Baloukas, O. Zabeida, J.E. Klemberg-Sapieha, L. Martinu, HiPIMS-deposited thermochromic VO₂ films on polymeric substrates, *Sol. Energy Mater. Sol. Cells* 155 (Oct. 2016) 60–69, <https://doi.org/10.1016/j.solmat.2016.04.048>.
- [26] J. Višniakov, A. Janulevičius, A. Maneikis, I. Matulaitienė, A. Selskis, S. Stanionytė, A. Suchodolskis, Antireflection TiO₂ coatings on textured surface grown by HiPIMS, *Thin Solid Films* 628 (Apr. 2017) 190–195, <https://doi.org/10.1016/j.tsf.2017.03.041>.
- [27] M. Burton, A. Palczewski, L. Phillips, A.M. Valente-Feliciano, C.E. Reece, RF results of Nb coated SRF accelerator cavities via hipims, in: 29th Linear Accelerator Conf, 2018, pp. 427–430, <https://doi.org/10.18429/JACoW-LINAC2018-TUP0042>.
- [28] A.M. Engwall, L.B. Bayu Aji, A.A. Baker, S.J. Shin, J.H. Bae, S.K. McCall, J. D. Moody, S.O. Kucheyev, Effect of substrate tilt on sputter-deposited AuTa films, *Appl. Surf. Sci.* 547 (May 2021) 149010, <https://doi.org/10.1016/j.apsusc.2021.149010>.
- [29] R. Alvarez, C. Lopez-Santos, J. Parra-Barranco, V. Rico, A. Barranco, J. Cotrino, A. R. Gonzalez-Elipe, A. Palmero, Nanocolumnar growth of thin films deposited at oblique angles: beyond the tangent rule, *J. Vac. Sci. Technol. B, Nanotechnol. Microelectron. Mater. Process. Meas. Phenom.* 32 (4) (Jul. 2014) 041802, <https://doi.org/10.1116/1.4882877>.
- [30] G. Greczynski, I. Petrov, J.E. Greene, L. Hultman, Paradigm shift in thin-film growth by magnetron sputtering: from gas-ion to metal-ion irradiation of the growing film, *J. Vac. Sci. Technol. A* 37 (6) (2019), 060801, <https://doi.org/10.1116/1.5121226>.
- [31] G. Greczynski, J. Lu, J. Jensen, S. Bolz, W. Kölker, C. Schiffers, O. Lemmer, J. E. Greene, L. Hultman, A review of metal-ion-flux-controlled growth of metastable TiAlN by HIPIMS/DCMS co-sputtering, *Surf. Coatings Technol.* 257 (2014) 15–25, <https://doi.org/10.1016/j.surfcoat.2014.01.055>.
- [32] Q. Ma, L. Li, Y. Xu, J. Gu, L. Wang, Y. Xu, Effect of bias voltage on TiAlSiN nanocomposite coatings deposited by HiPIMS, *Appl. Surf. Sci.* 392 (Jan. 2017) 826–833, <https://doi.org/10.1016/j.apsusc.2016.09.028>.
- [33] J.-F. Tang, C.-Y. Lin, F.-C. Yang, C.-L. Chang, Effects of input power ratio of AlCrTi target on the microstructural and mechanical properties of AlTiCrN coatings synthesized by a high-power impulse magnetron sputtering process, *Coatings* 11 (7) (Jul. 2021) 826, <https://doi.org/10.3390/coatings11070826>.

- [34] L.-C. Chang, C.-E. Wu, T.-Y. Ou, Mechanical properties and diffusion barrier performance of CrWN coatings fabricated through hybrid HIPIMS/RFMS, *Coatings* 11 (6) (Jun. 2021) 690, <https://doi.org/10.3390/coatings11060690>.
- [35] H. Fager, O. Tengstrand, J. Lu, S. Bolz, B. Mesic, W. Kölker, C. Schiffers, O. Lemmer, J.E. Greene, L. Hultman, I. Petrov, G. Greczynski, Low-temperature growth of dense and hard Ti_{0.41}Al_{0.51}Ta_{0.08}N films via hybrid HIPIMS/DC magnetron co-sputtering with synchronized metal-ion irradiation, *J. Appl. Phys.* 121 (17) (2017) 0–7, <https://doi.org/10.1063/1.4977818>.
- [36] C.A. Davis, A simple model for the formation of compressive stress in thin films by ion bombardment, *Thin Solid Films* 226 (1) (Apr. 1993) 30–34, [https://doi.org/10.1016/0040-6090\(93\)90201-Y](https://doi.org/10.1016/0040-6090(93)90201-Y).
- [37] E. Conwell, V.F. Weisskopf, Theory of impurity scattering in semiconductors, *Phys. Rev.* 77 (3) (Feb. 1950) 388–390, <https://doi.org/10.1103/PhysRev.77.388>.
- [38] R.N. Hall, Electron-hole recombination in germanium, *Phys. Rev.* 87 (2) (Jul. 1952) 387, <https://doi.org/10.1103/PhysRev.87.387>.
- [39] W. Shockley, W.T. Read, Statistics of the recombinations of holes and electrons, *Phys. Rev.* 87 (5) (Sep. 1952) 835–842, <https://doi.org/10.1103/PhysRev.87.835>.
- [40] G. Greczynski, J. Lu, M.P. Johansson, J. Jensen, I. Petrov, J.E. Greene, L. Hultman, Role of Ti⁺ and Alⁿ⁺ ion irradiation (n=1, 2) during Ti_{1-x}Al_xN alloy film growth in a hybrid HIPIMS/magnetron mode, *Surf. Coatings Technol.* 206 (19–20) (May 2012) 4202–4211, <https://doi.org/10.1016/j.surfcoat.2012.04.024>.
- [41] G. Greczynski, J. Lu, M. Johansson, J. Jensen, I. Petrov, J.E. Greene, L. Hultman, Selection of metal ion irradiation for controlling Ti_{1-x}Al_xN alloy growth via hybrid HIPIMS/magnetron co-sputtering, *Vacuum* 86 (8) (2012) 1036–1040, <https://doi.org/10.1016/j.vacuum.2011.10.027>.
- [42] C. Huo, M.A. Raadu, D. Lundin, J.T. Gudmundsson, A. Anders, N. Brenning, Gas rarefaction and the time evolution of long high-power impulse magnetron sputtering pulses, *Plasma Sources Sci. Technol.* 21 (4) (Aug. 2012) 045004, <https://doi.org/10.1088/0963-0252/21/4/045004>.
- [43] S.M. Rosnagel, Gas density reduction effects in magnetrons, *J. Vac. Sci. Technol. A Vacuum, Surfaces, Film.* 6 (1) (1988) 19–24, <https://doi.org/10.1116/1.574988>.
- [44] A. Palmero, H. Rudolph, F.H.P.M. Habraken, Study of the gas rarefaction phenomenon in a magnetron sputtering system, *Thin Solid Films* 515 (2) (Oct. 2006) 631–635, <https://doi.org/10.1016/j.tsf.2005.12.225>.
- [45] G. Greczynski, I. Zhirkov, I. Petrov, J.E. Greene, J. Rosen, Gas rarefaction effects during high power pulsed magnetron sputtering of groups IVB and VIB transition metals in Ar, *J. Vac. Sci. Technol. A Vacuum, Surfaces, Film.* 35 (6) (2017) 060601, <https://doi.org/10.1116/1.4989674>.
- [46] G. Greczynski, J. Lu, J. Jensen, I. Petrov, J.E. Greene, S. Bolz, W. Kölker, C. Schiffers, O. Lemmer, L. Hultman, Metal versus rare-gas ion irradiation during Ti_{1-x}Al_xN film growth by hybrid high power pulsed magnetron/dc magnetron co-sputtering using synchronized pulsed substrate bias, *J. Vac. Sci. Technol. A Vacuum, Surfaces, Film.* 30 (6) (2012) 061504, <https://doi.org/10.1116/1.4750485>.
- [47] N. Nedfors, O. Vozniy, J. Rosen, Effect of synchronized bias in the deposition of TiB₂ thin films using high power impulse magnetron sputtering, *J. Vac. Sci. Technol. A Vacuum, Surfaces, Film.* 36 (3) (May 2018) 031510, <https://doi.org/10.1116/1.5003194>.
- [48] R.P.B. Viloan, U. Helmersson, D. Lundin, Copper thin films deposited using different ion acceleration strategies in HIPIMS, *Surf. Coatings Technol.* 422 (Sep. 2021) 127487, <https://doi.org/10.1016/j.surfcoat.2021.127487>.
- [49] G. Greczynski, S. Mráz, J.M. Schneider, L. Hultman, Metal-ion sputter: a game changer for controlling nanostructure and phase formation during film growth by physical vapor deposition, *J. Appl. Phys.* 127 (18) (2020), <https://doi.org/10.1063/1.5141342>.
- [50] K. Hashimoto, Thin films deposition for BAW devices, in: *RF Bulk Acoustic Wave Filters for Communications*, Artech House, Norwood MA, 2009, pp. 174–175.
- [51] R. Farrell, V.R. Pagán, A. Kabulski, S. Kuchibhatla, J. Harman, K.R. Kasarla, L. E. Rodak, J. Hensel, P. Famouri, D. Korakakis, High temperature annealing studies on the piezoelectric properties of thin aluminum nitride films, *MRS Proc.* 1052 (Feb. 2007), <https://doi.org/10.1557/PROC-1052-DD06-18>, pp. 1052-DD06-18.
- [52] T. Aubert, M.B. Assouar, O. Legrani, O. Elmazria, C. Tiusan, S. Robert, Highly textured growth of AlN films on sapphire by magnetron sputtering for high temperature surface acoustic wave applications, *J. Vac. Sci. Technol. A Vacuum, Surfaces, Film.* 29 (2) (Mar. 2011) 021010, <https://doi.org/10.1116/1.3551604>.
- [53] B. Riahi, A. Ayad, J. Camus, M. Rammal, F. Boukari, L. Chekour, M.A. Djouadi, N. Rouag, Textured hexagonal and cubic phases of AlN films deposited on Si (100) by DC magnetron sputtering and high power impulse magnetron sputtering, *Thin Solid Films* 655 (Jun. 2018) 34–40, <https://doi.org/10.1016/j.tsf.2018.03.076>.
- [54] A.N. Red'kin, M.V. Ryzhova, E.E. Yakimov, D.V. Roshchupkin, Investigation of textured aluminum nitride films prepared by chemical vapor deposition, *Russ. Microelectron.* 46 (1) (Jan. 2017) 26–29, <https://doi.org/10.1134/S1063739717010085>.
- [55] N.A. Strnad, W.L. Sarney, G.B. Rayner, R.R. Benoit, G.R. Fox, R.Q. Rudy, T. J. Larrabee, J. Shallenberger, J.S. Pulskamp, Plasma enhanced atomic layer deposition of textured aluminum nitride on platinumized substrates for MEMS, *J. Vac. Sci. Technol. A* 40 (4) (Jul. 2022), 042403, <https://doi.org/10.1116/6.0001633>.
- [56] G. Zhou, L. Wang, X. Wang, Y. Yu, Influence of magnetic field configuration on plasma characteristics and thin film properties in dual magnetron reactive high power impulse magnetron sputtering discharge with Al in Ar/O₂ mixture, *Surf. Coatings Technol.* 409 (October 2020) (2021) 126837, <https://doi.org/10.1016/j.surfcoat.2021.126837>.
- [57] M. Zlatanović, R. Beloševac, A. Kunosić, Influence of magnetic field configuration on the deposition conditions in an unbalanced magnetron system, *Surf. Coatings Technol.* 90 (1–2) (1997) 143–149, [https://doi.org/10.1016/S0257-8972\(96\)03110-6](https://doi.org/10.1016/S0257-8972(96)03110-6).
- [58] V. Stranak, H. Wulff, R. Bogdanowicz, S. Drache, Z. Hubicka, M. Cada, M. Tichy, R. Hippler, Growth and properties of Ti-Cu films with respect to plasma parameters in dual-magnetron sputtering discharges, *Eur. Phys. J. D* 64 (2–3) (Oct. 2011) 427–435, <https://doi.org/10.1140/epjd/e2011-20393-7>.
- [59] V. Stranak, H. Wulff, P. Ksirova, C. Zietz, S. Drache, M. Cada, Z. Hubicka, R. Bader, M. Tichy, C.A. Helm, R. Hippler, Ionized vapor deposition of antimicrobial Ti-Cu films with controlled copper release, *Thin Solid Films* 550 (Jan. 2014) 389–394, <https://doi.org/10.1016/j.tsf.2013.11.001>.
- [60] V. Stranak, S. Drache, M. Cada, Z. Hubicka, M. Tichy, R. Hippler, Time-resolved diagnostics of dual high power impulse magnetron sputtering with pulse delays of 15 μs and 500 μs, *Contrib. to Plasma Phys.* 51 (2–3) (Mar. 2011) 237–245, <https://doi.org/10.1002/ctpp.201000065>.
- [61] G. Zhou, L. Wang, X. Wang, Y. Yu, Deposition of nanostructured crystalline alumina thin film by twin targets reactive high power impulse magnetron sputtering, *Appl. Surf. Sci.* 455 (Oct. 2018) 310–317, <https://doi.org/10.1016/j.apsusc.2018.05.153>.
- [62] M. Trant, M. Fischer, K. Thorwarth, S. Gauter, J. Patscheider, H.J. Hug, Tunable ion flux density and its impact on AlN thin films deposited in a confocal DC magnetron sputtering system, *Surf. Coatings Technol.* 348 (Aug. 2018) 159–167, <https://doi.org/10.1016/j.surfcoat.2018.04.091>.
- [63] J. Musil, P. Baroch, Discharge in dual magnetron sputtering system, *IEEE Trans. Plasma Sci.* 33 (2) (Apr. 2005) 338–339, <https://doi.org/10.1109/TPS.2005.844996>.
- [64] P. Baroch, J. Musil, Plasma Drift in Dual Magnetron Discharge, *IEEE Trans. Plasma Sci.* 36 (4) (Aug. 2008) 1412–1413, <https://doi.org/10.1109/TPS.2008.924483>.
- [65] S.K. Karkari, H. B. SaumlScker, D. Forster, J.W. Bradley, A technique for obtaining time- and energy-resolved mass spectroscopic measurements on pulsed plasmas, *Meas. Sci. Technol.* 13 (9) (Sep. 2002) 308, <https://doi.org/10.1088/0957-0233/13/9/308>.
- [66] S.A. Voronin, M.R. Alexander, J.W. Bradley, Time-resolved measurements of the ion energy distribution function in a pulsed discharge using a double gating technique, *Meas. Sci. Technol.* 16 (12) (Dec. 2005) 2446–2452, <https://doi.org/10.1088/0957-0233/16/12/007>.
- [67] J. Portillo, E.F. Rauch, S. Nicolopoulos, M. Gemmi, D. Bultreys, Precession electron diffraction assisted orientation mapping in the transmission electron microscope, *Mater. Sci. Forum* 644 (Mar. 2010) 1–7, <https://doi.org/10.4028/www.scientific.net/MSF.644.1>.
- [68] J. Alami, Plasma Characterization & Thin Film Growth and Analysis in Highly Ionized Magnetron Sputtering, Linköping University, 2005 [Online]. Available: <https://www.diva-portal.org/smash/get/diva2:20537/FULLTEXT01.pdf>.
- [69] P. Moskovkin, C. Maszl, R. Schierholz, W. Breilmann, J. Petersen, A. Pflug, J. Muller, M. Raza, S. Konstantinidis, A. von Keudell, S. Lucas, Link between plasma properties with morphological, structural and mechanical properties of thin Ti films deposited by high power impulse magnetron sputtering, *Surf. Coatings Technol.* 418 (Jul. 2021) 127235, <https://doi.org/10.1016/j.surfcoat.2021.127235>.
- [70] S.M. Borah, Direct current magnetron glow discharge plasma characteristics study for controlled deposition of titanium nitride thin film, *J. Mater.* 2013 (May 2013) 1–6, <https://doi.org/10.1155/2013/852859>.
- [71] G. Greczynski, I. Zhirkov, I. Petrov, J.E. Greene, J. Rosen, Control of the metal/gas ion ratio incident at the substrate plane during high-power impulse magnetron sputtering of transition metals in Ar, *Thin Solid Films* 642 (August) (2017) 36–40, <https://doi.org/10.1016/j.tsf.2017.09.027>.
- [72] M. Aiempnanakit, U. Helmersson, A. Aijaz, P. Larsson, R. Magnusson, J. Jensen, T. Kubart, Effect of peak power in reactive high power impulse magnetron sputtering of titanium dioxide, *Surf. Coatings Technol.* 205 (20) (Jul. 2011) 4828–4831, <https://doi.org/10.1016/j.surfcoat.2011.04.071>.
- [73] P.Y. Jouan, L. Le Brizoual, M. Ganciu, C. Cardinaud, S. Tricot, M.A. Djouadi, HIPIMS ion energy distribution measurements in reactive mode, *IEEE Trans. Plasma Sci.* 38 (11 PART 1) (2010) 3089–3094, <https://doi.org/10.1109/TPS.2010.2073688>.
- [74] M. Kitabatake, P. Fons, J.E. Greene, Molecular dynamics simulations of low-energy particle bombardment effects during vapor-phase crystal growth: 10 eV Si atoms incident on Si(001)2×1 surfaces, *J. Vac. Sci. Technol. A Vacuum, Surfaces, Film.* 8 (5) (Sep. 1990) 3726–3735, <https://doi.org/10.1116/1.576486>.
- [75] T.B.M. Charles, S. Barrett, *Structure of Metals: Crystallographic Methods, Principles and Data*, Pergamon Press, Oxford, 1980.
- [76] J.S. Cherg, C.M. Lin, T.Y. Chen, Two-step reactive sputtering of piezoelectric AlN thin films, *Surf. Coatings Technol.* 202 (22–23) (Aug. 2008) 5684–5687, <https://doi.org/10.1016/j.surfcoat.2008.06.087>.
- [77] J. Wang, Q. Zhang, G.F. Yang, C.J. Yao, Y.J. Li, R. Sun, J.L. Zhao, S.M. Gao, Effect of substrate temperature and bias voltage on the properties in DC magnetron sputtered AlN films on glass substrates, *J. Mater. Sci. Mater. Electron.* 27 (3) (Mar. 2016) 3026–3032, <https://doi.org/10.1007/s10854-015-4125-6>.
- [78] Y.-C. Yang, C.-T. Chang, Y.-C. Hsiao, J.-W. Lee, B.-S. Lou, Influence of high power impulse magnetron sputtering pulse parameters on the properties of aluminum nitride coatings, *Surf. Coatings Technol.* 259 (Nov. 2014) 219–231, <https://doi.org/10.1016/j.surfcoat.2014.05.028>.
- [79] P.F. Willemse, B.P. Naughton, Effect of small drawing reductions on residual surface stresses in thin cold-drawn steel wire, as measured by X-ray diffraction, *Mater. Sci. Technol.* 1 (1) (Jan. 1985) 41–44, <https://doi.org/10.1179/mst.1985.1.1.41>.
- [80] V. Hauk, R. Oudelhoven, Eigenspannungsanalyse an kaltgewalztem Nickel, *Int. J. Mater. Res.* 79 (1) (Jan. 1988) 41–49, <https://doi.org/10.1515/ijmr-1988-790107>.

- [81] G. Lorenzin, L.P.H. Jeurgens, C. Cancellieri, Stress tuning in sputter-grown Cu and W films for Cu/W nanomultilayer design, *J. Appl. Phys.* 131 (22) (Jun. 2022) 225304, <https://doi.org/10.1063/5.0088203>.
- [82] L.E. Koutsokeras, G. Abadias, Intrinsic stress in ZrN thin films: evaluation of grain boundary contribution from in situ wafer curvature and ex situ x-ray diffraction techniques, *J. Appl. Phys.* 111 (9) (May 2012) 093509, <https://doi.org/10.1063/1.4710530>.
- [83] E. Valcheva, J. Birch, P.O.Å. Persson, S. Tungasmita, L. Hultman, Epitaxial growth and orientation of AlN thin films on Si(001) substrates deposited by reactive magnetron sputtering, *J. Appl. Phys.* 100 (12) (Dec. 2006) 123514, <https://doi.org/10.1063/1.2402971>.
- [84] J. Xi, B. Liu, Y. Zhang, W.J. Weber, Ab initio molecular dynamics simulations of AlN responding to low energy particle radiation, *J. Appl. Phys.* 123 (4) (Jan. 2018) 045904, <https://doi.org/10.1063/1.5009750>.
- [85] F. Cemin, G. Abadias, T. Minea, D. Lundin, Tuning high power impulse magnetron sputtering discharge and substrate bias conditions to reduce the intrinsic stress of TiN thin films, *Thin Solid Films* 688 (Oct. 2019) 137335, <https://doi.org/10.1016/j.tsf.2019.05.054>.
- [86] T. Shimizu, K. Takahashi, R. Boyd, R.P. Viloan, J. Keraudy, D. Lundin, M. Yang, U. Helmersson, Low temperature growth of stress-free single phase α -W films using HiPIMS with synchronized pulsed substrate bias, *J. Appl. Phys.* 129 (15) (2021), <https://doi.org/10.1063/5.0042608>.
- [87] V. Lebedev, J. Jinschek, U. Kaiser, B. Schröter, W. Richter, J. Kräußlich, Epitaxial relationship in the AlN/Si(001) heterosystem, *Appl. Phys. Lett.* 76 (15) (Apr. 2000) 2029–2031, <https://doi.org/10.1063/1.126244>.